Interacting plasmonic nanostructures beyond the quasi-static limit: a "circuit" model

Xuezhi Zheng,[1,*] Niels Verellen,[2,3] Vladimir Volskiy,[1] Ventsislav K. Valev,[4] Jeremy J. Baumberg,[4] Guy A. E. Vandenbosch,[1] and Victor V. Moshchalkov[2]

[1]*Department of Electrical Engineering (ESAT-TELEMIC), KU Leuven, Kasteelpark Arenberg 10 bus 2444, 3001, Leuven, Belgium*

[2]*Institute for Nanoscale Physics and Chemistry (INPAC), KU Leuven, Celestijnenlaan 200D, 3001, Leuven, Belgium*

[3]*IMEC, Kapeldreef 75, 3001, Leuven, Belgium*

[4]*NanoPhotonics Centre, Cavendish Laboratory, Department of Physics, University of Cambridge, J. J. Thomson Avenue, Cambridge, CB30HE, UK*

[*]*xuezhi.zheng@esat.kuleuven.be*

Abstract: The interaction between individual plasmonic nanoparticles plays a crucial role in tuning and shaping the surface plasmon resonances of a composite structure. Here, we demonstrate that the detailed character of the coupling between plasmonic structures can be captured by a modified "circuit" model. This approach is generally applicable and, as an example here, is applied to a *dolmen*-like nanostructure consisting of a vertically placed gold *monomer* slab and two horizontally placed *dimer* slabs. By utilizing the full-wave eigenmode expansion method (EEM), we extract the eigenmodes and eigenvalues for these constituting elements and reduce their electromagnetic interaction to the structures' mode interactions. Using the reaction concept, we further summarize the mode interactions within a "coupling" matrix. When the driving voltage source imposed by the incident light is identified, an equivalent circuit model can be constructed. Within this model, hybridization of the plasmonic modes in the constituting nanostructure elements is discussed. The proposed circuit model allows the reuse of powerful circuit analysis techniques in the context of plasmonic structures. As an example, we derive an equivalent of Thévenin's theorem in circuit theory for nanostructures. Applying the equivalent Thévenin's theorem, the well-known Fano resonance is easily explained.

OCIS codes: (240.6680) Surface plasmons; (250.5403) Plasmonics; (310.6628) Subwavelength structures, nanostructures; (310.6805) Theory and design.

References and links

1. K. Aslan, J. R. Lakowicz, and C. D. Geddes, "Plasmon light scattering in biology and medicine: new sensing approaches, visions and perspectives," Curr. Opin. Chem. Biol. **9**(5), 538–544 (2005).
2. S. Nie and S. R. Emory, "Probing single molecules and single nanoparticles by surface-enhanced Raman scattering," Science **275**(5303), 1102–1106 (1997).
3. L. R. Hirsch, R. J. Stafford, J. A. Bankson, S. R. Sershen, B. Rivera, R. E. Price, J. D. Hazle, N. J. Halas, and J. L. West, "Nanoshell-mediated near-infrared thermal therapy of tumors under magnetic resonance guidance," Proc. Natl. Acad. Sci. U. S. A. **100**(23), 13549–13554 (2003).
4. N. Verellen, P. Van Dorpe, C. Huang, K. Lodewijks, G. A. E. Vandenbosch, L. Lagae, and V. V. Moshchalkov, "Plasmon line shaping using nanocrosses for high sensitivity localized surface plasmon resonance sensing," Nano Lett. **11**(2), 391–397 (2011).
5. N. Engheta, A. Salandrino, and A. Alù, "Circuit elements at optical frequencies: nanoinductors, nanocapacitors, and nanoresistors," Phys. Rev. Lett. **95**(9), 095504 (2005).
6. A. Alù, M. E. Young, and N. Engheta, "Design of nanofilters for optical nanocircuits," Phys. Rev. B **77**(14), 144107 (2008).
7. A. Alù and N. Engheta, "Input impedance, nanocircuit loading, and radiation tuning of optical nanoantennas," Phys. Rev. Lett. **101**(4), 043901 (2008).
8. V. K. Valev, A. V. Silhanek, B. De Clercq, W. Gillijns, Y. Jeyaram, X. Zheng, V. Volskiy, O. A. Aktsipetrov, G. A. E. Vandenbosch, M. Ameloot, V. V. Moshchalkov, and T. Verbiest, "U-shaped switches for optical information processing at the nanoscale," Small **7**(18), 2573–2576 (2011).

#199641 - $15.00 USD Received 17 Oct 2013; revised 27 Nov 2013; accepted 27 Nov 2013; published 10 Dec 2013

9. T. S. Troutman, J. K. Barton, and M. Romanowski, "Optical coherence tomography with plasmon resonant nanorods of gold," Opt. Lett. **32**(11), 1438–1440 (2007).
10. V. K. Valev, W. Libaers, U. Zywietz, X. Zheng, M. Centini, N. Pfullmann, L. O. Herrmann, C. Reinhardt, V. Volskiy, A. V. Silhanek, B. N. Chichkov, C. Sibilia, G. A. Vandenbosch, V. V. Moshchalkov, J. J. Baumberg, and T. Verbiest, "Nanostripe length dependence of plasmon-induced material deformations," Opt. Lett. **38**(13), 2256–2258 (2013).
11. F. Hao, C. L. Nehl, J. H. Hafner, and P. Nordlander, "Plasmon resonances of a gold nanostar," Nano Lett. **7**(3), 729–732 (2007).
12. V. K. Valev, B. D. Clercq, X. Zheng, D. Denkova, E. J. Osley, S. Vandendriessche, A. V. Silhanek, V. Volskiy, P. A. Warburton, G. A. Vandenbosch, M. Ameloot, V. V. Moshchalkov, and T. Verbiest, "The role of chiral local field enhancements below the resolution limit of Second Harmonic Generation microscopy," Opt. Express **20**(1), 256–264 (2012).
13. S. Linden, C. Enkrich, M. Wegener, J. Zhou, T. Koschny, and C. M. Soukoulis, "Magnetic response of metamaterials at 100 terahertz," Science **306**(5700), 1351–1353 (2004).
14. J. Aizpurua, P. Hanarp, D. S. Sutherland, M. Käll, G. W. Bryant, and F. J. García de Abajo, "Optical properties of gold nanorings," Phys. Rev. Lett. **90**(5), 057401 (2003).
15. V. K. Valev, B. De Clercq, C. G. Biris, X. Zheng, S. Vandendriessche, M. Hojeij, D. Denkova, Y. Jeyaram, N. C. Panoiu, Y. Ekinci, A. V. Silhanek, V. Volskiy, G. A. E. Vandenbosch, M. Ameloot, V. V. Moshchalkov, and T. Verbiest, "Distributing the optical near-field for efficient field-enhancements in nanostructures," Adv. Mater. **24**(35), OP208–OP215 (2012).
16. E. Prodan, C. Radloff, N. J. Halas, and P. Nordlander, "A hybridization model for the plasmon response of complex nanostructures," Science **302**(5644), 419–422 (2003).
17. S. Zhang, D. A. Genov, Y. Wang, M. Liu, and X. Zhang, "Plasmon-induced transparency in metamaterials," Phys. Rev. Lett. **101**(4), 047401 (2008).
18. P. K. Jain, K. S. Lee, I. H. El-Sayed, and M. A. El-Sayed, "Calculated absorption and scattering properties of gold nanoparticles of different size, shape, and composition: applications in biological imaging and biomedicine," J. Phys. Chem. B **110**(14), 7238–7248 (2006).
19. A. Alú, A. Salandrino, and N. Engheta, "Coupling of optical lumped nanocircuit elements and effects of substrates," Opt. Express **15**(21), 13865–13876 (2007).
20. I. D. Mayergoyz, D. R. Fredkin, and Z. Zhang, "Electrostatic (plasmon) resonances in nanoparticles," Phys. Rev. B **72**(15), 155412 (2005).
21. T. J. Davis, K. C. Vernon, and D. E. Gómez, "Designing plasmonic systems using optical coupling between nanoparticles," Phys. Rev. B **79**(15), 155423 (2009).
22. T. J. Davis, D. E. Gómez, and K. C. Vernon, "Simple model for the hybridization of surface plasmon resonances in metallic nanoparticles," Nano Lett. **10**(7), 2618–2625 (2010).
23. G. Mie, "Beiträge zur Optik trüber Medien, speziell kolloidaler Metallösungen," Ann. Phys. **330**(3), 377–445 (1908).
24. F. Papoff and B. Hourahine, "Geometrical Mie theory for resonances in nanoparticles of any shape," Opt. Express **19**(22), 21432–21444 (2011).
25. B. Hourahine and F. Papoff, "The geometrical nature of optical resonances: from a sphere to fused dimer nanoparticles," Meas. Sci. Technol. **23**(8), 084002 (2012).
26. C. E. Baum, "Emerging technology for transient and broadband analysis and synthesis of antennas and scatterers," Proc. IEEE **64**(11), 1598–1616 (1976).
27. G. A. E. Vandenbosch and A. R. Van de Capelle, "Mixed-potential integral expression formulation of the electric field in a stratified dielectric medium-application to the case of a probe current source," IEEE Trans. Antennas Propag. **40**(7), 806–817 (1992).
28. F. J. Demuynck, G. A. E. Vandenbosch, and A. R. Van de Capelle, "The expansion wave concept–Part I: Efficient calculation of spatial Green's functions in a stratified dielectric medium," IEEE Trans. Antennas Propag. **46**, 397–406 (1998).
29. Y. Schols and G. A. E. Vandenbosch, "Separation of horizontal and vertical dependencies in a surface/volume integral equation approach to model quasi 3-D structures in multilayered media," IEEE Trans. Antennas Propag. **55**(4), 1086–1094 (2007).
30. G. A. E. Vandenbosch, V. Volski, N. Verellen, and V. V. Moshchalkov, "On the use of the method of moments in plasmonic applications," Radio Sci. **46**(5), RS0E02 (2011).
31. V. H. Rumsey, "Reaction concept in electromagnetic theory," Phys. Rev. **94**(6), 1483–1491 (1954).
32. C. G. Montgomery, R. H. Dicke, and E. M. Purcell, *Principles of Microwave Circuits* (IET, 1948).
33. N. Verellen, Y. Sonnefraud, H. Sobhani, F. Hao, V. V. Moshchalkov, P. Van Dorpe, P. Nordlander, and S. A. Maier, "Fano resonances in individual coherent plasmonic nanocavities," Nano Lett. **9**(4), 1663–1667 (2009).
34. U. Fano, "Effects of configuration interaction on intensities and phase shifts," Phys. Rev. **124**(6), 1866–1878 (1961).
35. B. Gallinet and O. J. Martin, "*Ab initio* theory of Fano resonances in plasmonic nanostructures and metamaterials," Phys. Rev. B **83**(23), 235427 (2011).
36. B. Gallinet and O. J. Martin, "Influence of electromagnetic interactions on the line shape of plasmonic Fano resonances," ACS Nano **5**(11), 8999–9008 (2011).
37. V. Giannini, Y. Francescato, H. Amrania, C. C. Phillips, and S. A. Maier, "Fano resonances in nanoscale plasmonic systems: a parameter-free modeling approach," Nano Lett. **11**(7), 2835–2840 (2011).
38. Y. Francescato, V. Giannini, and S. A. Maier, "Plasmonic systems unveiled by Fano resonances," ACS Nano **6**(2), 1830–1838 (2012).

#199641 - $15.00 USD Received 17 Oct 2013; revised 27 Nov 2013; accepted 27 Nov 2013; published 10 Dec 2013

39. A. Lovera, B. Gallinet, P. Nordlander, and O. J. Martin, "Mechanisms of Fano resonances in coupled plasmonic systems," ACS Nano **7**(5), 4527–4536 (2013).
40. G. W. Hanson and A. B. Yakovlev, *Operator Theory for Electromagnetics: An Introduction* (Springer, 2002).
41. A. G. Ramm, "Mathematical foundations of the singularity and eigenmode expansion methods (SEM and EEM)," J. Math. Anal. Appl. **86**(2), 562–591 (1982).
42. R. F. Harrington, *Field Computation by Moment Methods* (IEEE, 1993).
43. X. Zheng, N. Verellen, V. K. Valev, V. Volskiy, D. Denkova, L. O. Herrmann, C. Blejean, J. J. Baumberg, A. V. Silhanek, G. A. E. Vandenbosch, and V. V. Moshchalkov, " Nanoantenna modeled as N-port network: bridging surface plasmon modes and nano-circuits," submitted (2013).
44. J. D. Jackson, *Classical Electrodynamics* (John Wiley, 1998).

1. Introduction

Localized surface plasmon resonances (LSPR) in nanoparticles have found many applications spanning from the realm of life sciences, including biomedicine, bio-sensing, cancer treatment [1–4], to the conventional research domain of electrical engineering, such as the design of nanocircuits, nanofilters and nanoantennas [5–8]. Modern nanofabrication techniques have allowed plasmonic properties to be a explored in a variety of topologies, such as rods [9,10], stars [11,12], split-rings [13], and rings [14,15], to name a few. With the nanoparticles closely spaced, the surface plasmons, i.e. the collective oscillations of conduction electrons, start to interact and, as a result, many exotic line features can be observed in the spectrum of the composite nanostructure, such as the splitting of the resonant frequencies [16] and spectral transparency known as plasmon induced transparency [17]. In order to predict the effects of mutual coupling between nanoparticles, several methods have been proposed on the ground of modal analysis (or Eigenmode Analysis). For example, by assuming the size of constituent nanoparticles much smaller than the wavelengths of the incident light, a dipole-interaction model is conceived and applied to the spectral splitting of nanoparticle pairs [18]. In the same spirit, the coupling between small nanoparticles is integrated into an optical lumped nanocircuit theory [19]. By considering the influence of higher order resonances, the coupling between surface plasmon modes is modeled by hybridization theory, similar to molecular hybridization theory where the atomic orbitals mix and form new molecular orbitals. Further, based on the nanoparticles' electrostatic resonances [20], a methodology of systematically designing and analyzing the optical properties of an ensemble of nanoparticles is presented in [21,22]. However, all these models are constructed within the quasi-static limit. It is known that for nanoparticles with larger dimensions, the retardation effects, i.e. the phase changes of the excitation field over the nanoparticle volume, cannot be neglected and a rigorous electrodynamic model is required. With the electromagnetic response of a particle expressed by a set of eigenmodes of scattering fields and internal fields, such size effects can be captured by the Mie theory for spheres [23] and the geometrical Mie theory for arbitrary particles without sharp edges [24,25].

In this work, in contrast to pursue the field eigenmodes which span the whole space, we especially focus on the current eigenmodes supported by arbitrary nanoparticles. We perform a *full-wave* Eigenmode Expansion Method [26] implemented in the framework of a Volumetric Method of Moments (V-MoM) Solution [27–30]. Utilizing a dolmen-like nanostructure (dimensions, materials and depth profile are shown in Fig. 1), we illustrate that in contrast to the electrostatic modal analysis [20] where the material contribution is the only factor affecting the resonances, in a *full-wave* eigenmode analysis the radiation, as the result of retardation effects, comes into the picture and plays a crucial role in determining the resonances of surface plasmon modes. Further, we extract the eigenmodes and eigenvalues of the dolmen's constituent structures: a monomer (single vertical gold slab with dimensions W1, L1 as shown in Fig. 1) and dimer (two parallel, horizontally aligned gold slabs with dimensions W2, L2 as shown in Fig. 1), and reduce the electromagnetic interaction between the monomer and the dimer to their eigenmodes' interaction. By making use of the reaction concept [31], the eigenmodes' interaction is simplified to an equivalent circuit model, based on which the hybridization of surface plasmon modes is discussed. Last but not least, the proposed circuit model enables the reuse of powerful circuit analysis techniques in the context of plasmonic applications. As an example, we develop an equivalent of Thevenin's theorem

#199641 - $15.00 USD Received 17 Oct 2013; revised 27 Nov 2013; accepted 27 Nov 2013; published 10 Dec 2013

[32] for composite nanostructures and use it to explain the well-known Fano interference [33–39] in the dolmen structure.

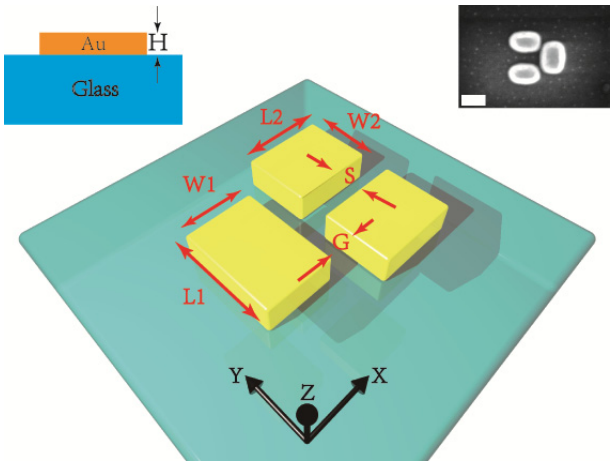

Fig. 1. Dolmen structure. The topology, the depth profile and SEM image of a gold dolmen nanostructure (L1 = 160 nm, W1 = 110 nm, L2 = 135 nm, W2 = 100 nm, S = 55 nm, G = 20 nm, H = 50 nm). The white bar in the SEM image represents 100 nm.

2. The eigenvalue problem for a nanoscatterer

In this section, the eigenvalue problem is formulated for a general electromagnetic scattering problem and specifically illustrated for monomer, dimer and dolmen structures. The eigenvalues and eigenmodes of the dolmen structure are numerically extracted and their relation to the plasmonic response is discussed. Throughout the rest of this work, the time dependency $e^{-i\omega t}$ is considered. The angular frequency of the oscillation is denoted by ω. Note that the substrate effect is always considered in the analysis.

Consider the interaction of electromagnetic waves with the dolmen nanostructure sitting on top of a glass substrate. At all space points, the total electric field $\mathbf{E}_{\text{tot}}(\mathbf{r},\omega)$ is the sum of the scattered $\mathbf{E}_{\text{scat}}(\mathbf{r},\omega)$ and the incident $\mathbf{E}_{\text{inc}}(\mathbf{r},\omega)$ electric fields,

$$\mathbf{E}_{\text{tot}}(\mathbf{r},\omega)=\mathbf{E}_{\text{inc}}(\mathbf{r},\omega)+\mathbf{E}_{\text{scat}}(\mathbf{r},\omega),\ \mathbf{r}\in \textit{entire space}. \tag{1}$$

In Eq. (1), the incident field $\mathbf{E}_{\text{inc}}(\mathbf{r},\omega)$ is the unperturbed field, i.e. the sum of the incoming plane wave and the reflected plane wave without the presence of nanostructures.

Specifically, in the monomer volume (V_M), the total field $\mathbf{E}_{\text{tot}}(\mathbf{r},\omega)$, due to the volume equivalence principle, is related with the total electric current $\mathbf{J}_{\mathbf{M}}(\mathbf{r},\omega)$ (including both conduction and displacement current),

$$\mathbf{E}_{\text{tot}}(\mathbf{r},\omega)=\frac{\mathbf{J}_{\mathbf{M}}(\mathbf{r},\omega)}{-i\omega\left(\varepsilon(\mathbf{r},\omega)-\varepsilon_0\right)},\ \mathbf{r}\in V_M. \tag{2}$$

The scattered field $\mathbf{E}_{\text{scat}}(\mathbf{r})$ in the monomer includes both the scattered field generated by the monomer and by the dimer,

#199641 - $15.00 USD Received 17 Oct 2013; revised 27 Nov 2013; accepted 27 Nov 2013; published 10 Dec 2013

$$\mathbf{E}_{\mathbf{scat}}(\mathbf{r},\omega) = -i\omega\mu_0 \int_{V_M} \overline{\mathbf{G}}_{\mathbf{MM}}(\mathbf{r},\mathbf{r}',\omega)\cdot\mathbf{J}_{\mathbf{M}}(\mathbf{r}',\omega)\,dv' - i\omega\mu_0 \int_{V_D} \overline{\mathbf{G}}_{\mathbf{MD}}(\mathbf{r},\mathbf{r}',\omega)\cdot\mathbf{J}_{\mathbf{D}}(\mathbf{r}',\omega)\,dv', \mathbf{r}\in V_M. \quad (3)$$

In Eqs. (2) and (3), ε_0 and μ_0 are the vacuum permittivity and the vacuum permeability, whereas $\varepsilon(\mathbf{r},\omega)$ describes the dielectric function of the material occupying the space volume of the monomer V_M. The tensor Green's functions $\overline{\mathbf{G}}_{\mathbf{MM}}(\mathbf{r},\mathbf{r}';\omega)$ and $\overline{\mathbf{G}}_{\mathbf{MD}}(\mathbf{r},\mathbf{r}';\omega)$ take the substrate effects into account and describe the self-coupling of the monomer and the mutual-coupling between the dimer and the monomer. The integration in the first term on the right hand side of Eq. (3) is carried out over the monomer nanoparticle (V_M), while in the second term this integration is over the volume of the dimer nanoparticle (V_D) excluding the air gap in between.

Similar relations for the dimer are given by

$$\mathbf{E}_{\mathbf{tot}}(\mathbf{r},\omega) = \frac{\mathbf{J}_{\mathbf{D}}(\mathbf{r},\omega)}{-i\omega\left(\varepsilon(\mathbf{r},\omega)-\varepsilon_0\right)}, \mathbf{r}\in V_D, \quad (4)$$

$$\mathbf{E}_{\mathbf{scat}}(\mathbf{r},\omega) = -i\omega\mu_0 \int_{V_D} \overline{\mathbf{G}}_{\mathbf{DD}}(\mathbf{r},\mathbf{r}',\omega)\cdot\mathbf{J}_{\mathbf{D}}(\mathbf{r}',\omega)\,dv' - i\omega\mu_0 \int_{V_M} \overline{\mathbf{G}}_{\mathbf{DM}}(\mathbf{r},\mathbf{r}',\omega)\cdot\mathbf{J}_{\mathbf{M}}(\mathbf{r}',\omega)\,dv', \mathbf{r}\in V_D. \quad (5)$$

Substituting Eqs. (2) and (3) and Eqs. (4) and (5) into Eq. (1), we can construct a system of equations,

$$C_{MM}\left(\mathbf{J}_{\mathbf{M}}(\mathbf{r}',\omega)\right) + C_{MD}\left(\mathbf{J}_{\mathbf{D}}(\mathbf{r}',\omega)\right) = \mathbf{E}_{\mathbf{inc}}(\mathbf{r},\omega), \mathbf{r}\in V_M, \quad (6)$$

$$C_{DM}\left(\mathbf{J}_{\mathbf{M}}(\mathbf{r}',\omega)\right) + C_{DD}\left(\mathbf{J}_{\mathbf{D}}(\mathbf{r}',\omega)\right) = \mathbf{E}_{\mathbf{inc}}(\mathbf{r},\omega), \mathbf{r}\in V_D. \quad (7)$$

The functional relations C_{MM}, C_{DD}, C_{MD} and C_{DM} are defined as,

$$C_{MM}\left(\mathbf{J}_{\mathbf{M}}(\mathbf{r}',\omega)\right) = \frac{\mathbf{J}_{\mathbf{M}}(\mathbf{r},\omega)}{-i\omega\left(\varepsilon(\mathbf{r},\omega)-\varepsilon_0\right)} + i\omega\mu_0 \int_{V_M} \overline{\mathbf{G}}_{\mathbf{MM}}(\mathbf{r},\mathbf{r}',\omega)\cdot\mathbf{J}_{\mathbf{M}}(\mathbf{r}',\omega)\,dv', \mathbf{r}\in V_M, \quad (8)$$

$$C_{DD}\left(\mathbf{J}_{\mathbf{D}}(\mathbf{r}',\omega)\right) = \frac{\mathbf{J}_{\mathbf{D}}(\mathbf{r},\omega)}{-i\omega\left(\varepsilon(\mathbf{r},\omega)-\varepsilon_0\right)} + i\omega\mu_0 \int_{V_D} \overline{\mathbf{G}}_{\mathbf{DD}}(\mathbf{r},\mathbf{r}',\omega)\cdot\mathbf{J}_{\mathbf{D}}(\mathbf{r}',\omega)\,dv', \mathbf{r}\in V_D, \quad (9)$$

$$C_{MD}\left(\mathbf{J}_{\mathbf{D}}(\mathbf{r}',\omega)\right) = i\omega\mu_0 \int_{V_D} \overline{\mathbf{G}}_{\mathbf{MD}}(\mathbf{r},\mathbf{r}',\omega)\cdot\mathbf{J}_{\mathbf{D}}(\mathbf{r}',\omega)\,dv', \mathbf{r}\in V_M, \quad (10)$$

$$C_{DM}\left(\mathbf{J}_{\mathbf{M}}(\mathbf{r}',\omega)\right) = i\omega\mu_0 \int_{V_M} \overline{\mathbf{G}}_{\mathbf{DM}}(\mathbf{r},\mathbf{r}',\omega)\cdot\mathbf{J}_{\mathbf{M}}(\mathbf{r}',\omega)\,dv', \mathbf{r}\in V_D. \quad (11)$$

For the functional relations C_{MM} and C_{DD}, the associated eigenvalue problems can be found,

$$C_{MM}\left|\mathbf{J}_{\mathbf{n}}^{M}(\mathbf{r},\omega)\right\rangle = \lambda_n^M(\omega)\left|\mathbf{J}_{\mathbf{n}}^{M}(\mathbf{r},\omega)\right\rangle, \mathbf{r}\in V_M, \quad (12)$$

$$C_{DD}\left|\mathbf{J}_{\mathbf{n}}^{D}(\mathbf{r},\omega)\right\rangle = \lambda_n^D(\omega)\left|\mathbf{J}_{\mathbf{n}}^{D}(\mathbf{r},\omega)\right\rangle, \mathbf{r}\in V_D. \quad (13)$$

The subscripts of $\left|\mathbf{J}_{\mathbf{n}}^{M}(\mathbf{r},\omega)\right\rangle$ and $\lambda_n^M(\omega)$ in Eq. (12) ($\left|\mathbf{J}_{\mathbf{n}}^{D}(\mathbf{r},\omega)\right\rangle$ and $\lambda_n^D(\omega)$ in Eq. (13)) denote the order of an eigenmode and its corresponding eigenvalue, while their superscripts represent which structure, e.g. the monomer or the dimer, the eigenmode and eigenvalue belong to. Due to the reciprocity of the Green's function, both C_{MM} and C_{DD} are complex

#199641 - $15.00 USD Received 17 Oct 2013; revised 27 Nov 2013; accepted 27 Nov 2013; published 10 Dec 2013

symmetric (non-Hermitian) operators. Their eigenfunctions $\left|\mathbf{J}_{\mathbf{n}}^{M}(\mathbf{r},\omega)\right\rangle$ and $\left|\mathbf{J}_{\mathbf{n}}^{D}(\mathbf{r},\omega)\right\rangle$ are complex and form a complex orthonormal set,

$$\begin{aligned}\left\langle \mathbf{J}_{\mathbf{m}}^{M}(\mathbf{r},\omega),\mathbf{J}_{\mathbf{n}}^{M}(\mathbf{r},\omega)\right\rangle &= \int_{V'}\mathbf{J}_{\mathbf{m}}^{M}(\mathbf{r},\omega)\cdot\mathbf{J}_{\mathbf{n}}^{M}(\mathbf{r},\omega)\,dv' = \begin{cases}1 & m=n\\ 0 & m\neq n\end{cases},\\ \left\langle \mathbf{J}_{\mathbf{m}}^{D}(\mathbf{r},\omega),\mathbf{J}_{\mathbf{n}}^{D}(\mathbf{r},\omega)\right\rangle &= \int_{V'}\mathbf{J}_{\mathbf{m}}^{D}(\mathbf{r},\omega)\cdot\mathbf{J}_{\mathbf{n}}^{D}(\mathbf{r},\omega)\,dv' = \begin{cases}1 & m=n\\ 0 & m\neq n\end{cases}.\end{aligned} \tag{14}$$

Moreover, when the volumes of the monomer (V_M) and dimer nanoparticles (V_D), i.e. the dolmen structure (V), are considered as a whole, Eqs. (6) and (7) can be summarized in a single equation,

$$C\left(\mathbf{J}(\mathbf{r},\omega)\right)=\mathbf{E}_{\mathbf{inc}}(\mathbf{r},\omega). \tag{15}$$

The functional relation in Eq. (15) is defined over the volume of dolmen V,

$$C\left(\mathbf{J}(\mathbf{r},\omega)\right)=\frac{\mathbf{J}(\mathbf{r},\omega)}{-i\omega\left(\varepsilon(\mathbf{r},\omega)-\varepsilon_0\right)}+i\omega\mu_0\int_{V}\overline{\mathbf{G}}(\mathbf{r},\mathbf{r}',\omega)\cdot\mathbf{J}(\mathbf{r},\omega)\,dv',\ \mathbf{r}\in V. \tag{16}$$

Similar to Eqs. (12) and (13), the associated eigenvalue problem can be defined and the eigenmodes form a complex orthogonal set,

$$\begin{aligned}C\left|\mathbf{J}_{\mathbf{n}}(\mathbf{r},\omega)\right\rangle &= \lambda_n(\omega)\left|\mathbf{J}_{\mathbf{n}}(\mathbf{r},\omega)\right\rangle,\ \mathbf{r}\in V,\\ \left\langle \mathbf{J}_{\mathbf{m}}(\mathbf{r},\omega),\mathbf{J}_{\mathbf{n}}(\mathbf{r},\omega)\right\rangle &= \int_{V'}\mathbf{J}_{\mathbf{m}}(\mathbf{r},\omega)\cdot\mathbf{J}_{\mathbf{n}}(\mathbf{r},\omega)\,dv' = \begin{cases}1 & m=n\\ 0 & m\neq n\end{cases}.\end{aligned} \tag{17}$$

As in [26], we assume that the eigenmodes $\left|\mathbf{J}_{\mathbf{n}}(\mathbf{r},\omega)\right\rangle$ in Eq. (17) form the basis for the Hilbert space. Thus, the solution to Eq. (15) can be represented by the linear combination of eigenmodes,

$$\mathbf{J}(\mathbf{r},\omega)=\sum_{n}c_n(\omega)\mathbf{J}_{\mathbf{n}}(\mathbf{r},\omega). \tag{18}$$

Since the operators defined in Eqs. (8) and (9) are not Hermitian but complex symmetric operators, the spectral theorem [40] does not apply. That is, there is no guarantee that solutions to the eigenvalue problems in Eqs. (12) and (13) always exist. Moreover, even in the case that Eqs. (12) and (13) do exist, in general, the root system [40,41] forms the basis, i.e. the complete set which spans the domain of the integral operator in Eqs. (6) and (7), rather than the complex orthonormal set in Eq. (14). Therefore, within the framework of operator theory there could be a problem with mathematical rigorousness.

However, in practice the integral operators with infinite dimensions in Eqs. (8) and (9) are always reduced to finite dimensions by, e.g., the Method of Moments algorithm [42], whereby an N x N matrix is obtained. Under such circumstances, if this matrix is diagonalizable and has distinct eigenvalues, an associated linearly independent set spanning the vector space can be found. Specifics on the mathematical background of this method can be found in [40] and [41]. By using the complex orthonormal relation in Eq. (17), the coupling coefficient $c_n(\omega)$ in (18) can be derived,

$$c_n(\omega)=\frac{\left\langle \mathbf{J}_{\mathbf{n}}(\mathbf{r},\omega),\ \mathbf{E}_{\mathbf{inc}}(\mathbf{r},\omega)\right\rangle}{\lambda_n(\omega)}. \tag{19}$$

In order to illustrate how the eigenmodes and eigenvalues determine the response of the dolmen structure, we extract its first five eigenmodes (indicated with L*n*), the corresponding eigenvalues, and their coupling to polarized incident light (See Fig. 2). In contrast to the L2 and L4 modes, the charges of the L1, L3 and L5 modes are mainly separated in the Y direction (see surface charge density distributions in inset Figs. 2(a) and 2(e)). Thus, the L1, L3 and L5 modes are better coupled with Y polarized light (See Figs. 2(c) and 2(g)). As found in [43], an eigenvalues' imaginary part is related with the difference between the power stored

#199641 - $15.00 USD Received 17 Oct 2013; revised 27 Nov 2013; accepted 27 Nov 2013; published 10 Dec 2013

in electric field and magnetic field generated by the corresponding eigenmode. Similar to an RLC circuit, the resonance of an eigenmode is reached whenever the electrically stored power balances the magnetically stored one. Thus, at the wavelength where the imaginary part of their eigenvalue crosses zero, the coupling of the L1, L3, and L5 modes to Y polarized light tends to approach a maximum (See the grey dashed vertical lines in Figs. 2(b) and 2(c)). The resonances of the L1, L3 and L5 modes are determined by further considering the effects of the eigenvalues' real part (as denoted by the arrows in Fig. 2(c)): the larger the eigenvalues' real part is, the more the resonance shifts from the wavelength where the imaginary part of the eigenvalue crosses zero. Note that this real part is related to the power lost via material dissipation and radiation by the eigenmodes' scattered fields [43]. Since the plasmonic material constituting the dolmen is always the same (gold), the difference in the eigenvalues' real part is attributed to the radiative loss. Consequently, from comparing the real part of the eigenvalues of L2 and L4 for example, we can conclude that the L2 mode is more radiative than the L4 mode. The same can be concluded for L1, L3 and L5, where now L5 is the most radiative one, L1 is less radiative, and L3 is the least radiative. This can also be observed from the experimental extinction spectra (Figs. 2(d) and 2(h)). Since L3 and L4 are less radiative, i.e. their net dipolar moments are relatively small, they are weakly coupled with the incident field. As a result, their plasmonic responses are overshadowed by the response of the brighter modes.

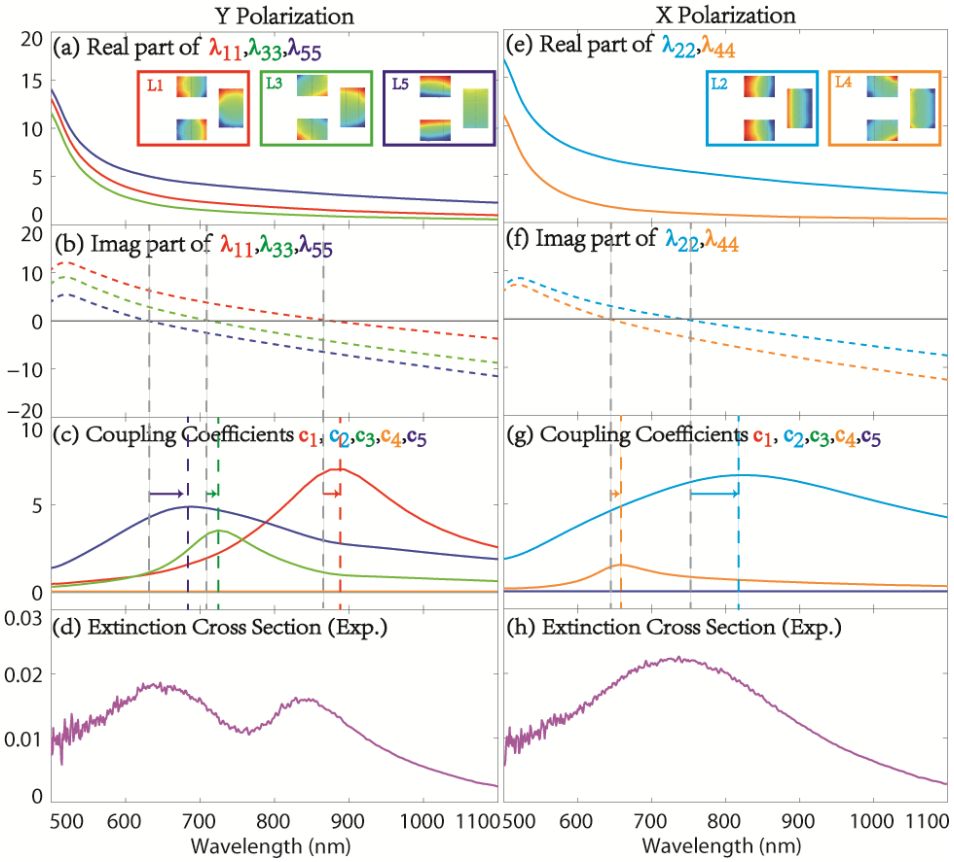

Fig. 2. Eigenmodes, eigenvalues and plasmonic response of the composite dolmen structure. The first five eigenmodes are extracted for the dolmen structure and their charge density distribution is shown in the insets of (a) for the L1, L3, and L5 modes and (e) for the L2 and L4 modes (blue and red indicate negative and positive charge, resp.). The real (solid) and the imaginary (dash) parts of their eigenvalues are presented in (a,e) and (b,f), resp. The coupling coefficients are shown in (c) and (g). The measured extinction cross sections of the dolmen structure are shown in (d) and (h) for Y and X polarized incident light, resp.

#199641 - $15.00 USD Received 17 Oct 2013; revised 27 Nov 2013; accepted 27 Nov 2013; published 10 Dec 2013

3. The hybridization between monomer and dimer eigenmodes: a "circuit" model

To illustrate the interaction between the monomer and the dimer, a simple case is considered, where the current $\mathbf{J}(\mathbf{r},\omega)$ induced by the Y polarized incident light is taken as a linear combination of the monomer's dipolar mode (See the inset in the rightmost column of Fig. 3(a)) and the dimer's quadrupolar mode which consists of two out-of-phase oscillating dipoles (See the inset in the leftmost column of Fig. 3(a)),

$$\mathbf{J}(\mathbf{r},\omega) = j_1^M(\omega)\mathbf{J}_1^M(\mathbf{r},\omega) + j_1^D(\omega)\mathbf{J}_1^D(\mathbf{r},\omega). \tag{20}$$

In Eq. (20), $j_1^M(\omega)$ and $j_1^D(\omega)$ denote the contributions from the monomer's dipolar mode $\mathbf{J}_1^M(\mathbf{r},\omega)$ and the dimer's quadrupolar mode $\mathbf{J}_1^D(\mathbf{r},\omega)$ to the induced current $\mathbf{J}(\mathbf{r},\omega)$ flowing in the dolmen structure. Substituting Eq. (20) into Eqs. (6) and (7), we can find that

$$C_{MM}\left(j_1^M(\omega)\mathbf{J}_1^M(\mathbf{r}',\omega)\right) + C_{MD}\left(j_1^D(\omega)\mathbf{J}_1^D(\mathbf{r}',\omega)\right) = \mathbf{E}_{\mathbf{inc}}(\mathbf{r},\omega), \mathbf{r}\in V_M, \tag{21}$$

$$C_{DM}\left(j_1^M(\omega)\mathbf{J}_1^M(\mathbf{r}',\omega)\right) + C_{DD}\left(j_1^D(\omega)\mathbf{J}_1^D(\mathbf{r}',\omega)\right) = \mathbf{E}_{\mathbf{inc}}(\mathbf{r},\omega), \mathbf{r}\in V_D. \tag{22}$$

Left-multiplying Eq. (21) (Eq. (22)) by $\mathbf{J}_1^M(\mathbf{r}',\omega)$ ($\mathbf{J}_1^D(\mathbf{r}',\omega)$) and integrating over the monomer's (dimer's) volume, we have

$$\begin{pmatrix} c^{MM}(\omega) & c^{MD}(\omega) \\ c^{DM}(\omega) & c^{DD}(\omega) \end{pmatrix}\begin{pmatrix} j_1^M(\omega) \\ j_1^D(\omega) \end{pmatrix} = \begin{pmatrix} e_1^M(\omega) \\ e_1^D(\omega) \end{pmatrix}. \tag{23}$$

Since the impedance matrix of a T-Network [32] is a 2 by 2 matrix such as the matrix on the left hand side of Eq. (23), we can conceive an equivalent circuit model (See Fig. 3(c)) for the interaction between the monomer's dipolar mode and the dimer's quadrupolar mode. The electromagnetic effects (e.g. self-coupling, mutual coupling, etc.) of the monomer's and dimer's fundamental modes are summarized within two coupled circuit loops, i.e. the "monomer" loop and the "dimer" loop.

The *self-coupling* of an eigenmode, i.e. the reaction [31] of a current eigenmode to the electric fields generated by itself, is described by $c^{MM}(\omega)$ for the "monomer" loop and by $c^{DD}(\omega)$ for the "dimer" loop (See the left and right graphs in Fig. 3(a)). Noticing the eigenvalue problems defined in Eqs. (12) and (13) and the orthogonality of eigenmodes in Eq. (14), we can find that $c^{MM}(\omega)$ and $c^{DD}(\omega)$ are actually the eigenvalues of the monomer's dipolar mode and the dimer's quadrupolar mode,

$$c^{MM}(\omega) = \int_{V_M} \mathbf{J}_1^M(\mathbf{r}',\omega)\cdot C_{MM}\left(\mathbf{J}_1^M(\mathbf{r}',\omega)\right)dv = \lambda_1^M(\omega), \tag{24}$$

$$c^{DD}(\omega) = \int_{V_D} \mathbf{J}_1^D(\mathbf{r}',\omega)\cdot C_{DD}\left(\mathbf{J}_1^D(\mathbf{r}',\omega)\right)dv = \lambda_1^D(\omega). \tag{25}$$

Similarly, $c^{MD}(\omega)$ and $c^{DM}(\omega)$ describe the *mutual coupling*, i.e. the reaction [31] of a current eigenmode to the electric fields generated by another current eigenmode, between the monomer's and the dimer's fundamental modes (See Fig. 3(b)),

$$c^{MD}(\omega) = \int_{V_D} \mathbf{J}_1^M(\mathbf{r}',\omega)\cdot C_{MD}\left(\mathbf{J}_1^D(\mathbf{r}',\omega)\right)dv, \tag{26}$$

$$c^{DM}(\omega) = \int_{V_D} \mathbf{J}_1^D(\mathbf{r}',\omega)\cdot C_{DM}\left(\mathbf{J}_1^M(\mathbf{r}',\omega)\right)dv. \tag{27}$$

Due to the reciprocity of Maxwell's equations, $c^{MD}(\omega)$ is equal to $c^{DM}(\omega)$. It is worth noticing that in order to numerically evaluate the functional relations in Eqs. (8)–(11) and in

#199641 - $15.00 USD Received 17 Oct 2013; revised 27 Nov 2013; accepted 27 Nov 2013; published 10 Dec 2013

Eq. (16), we can discretize the monomer (V_M) and the dimer (V_D) by hexahedral blocks and associate two adjacent blocks with a presumed local current distribution **f**(**r**) of unit amplitude, called *basis function*. By further applying a testing procedure, we can recast, for example, Eqs. (10) and (11) into a matrix form [29],

$$\left(C_{MD}\right)_{mn} = i\omega\mu_0 \int_V \mathbf{g}_{\mathbf{M}}^m\left(\mathbf{r}\right)\left[\int_{V'} \overline{\mathbf{G}}_{\mathbf{MD}}\left(\mathbf{r},\mathbf{r}',\omega\right)\cdot\mathbf{f}_{\mathbf{D}}^n\left(\mathbf{r}'\right)dv'\right]dv, \mathbf{r}'\in V_D, \mathbf{r}\in V_M, \quad (28)$$

$$\left(C_{DM}\right)_{mn} = i\omega\mu_0 \int_V \mathbf{g}_{\mathbf{D}}^m\left(\mathbf{r}\right)\left[\int_{V'} \overline{\mathbf{G}}_{\mathbf{DM}}\left(\mathbf{r},\mathbf{r}',\omega\right)\cdot\mathbf{f}_{\mathbf{M}}^n\left(\mathbf{r}'\right)dv'\right]dv, \mathbf{r}'\in V_M, \mathbf{r}\in V_D. \quad (29)$$

In Eqs. (28) and (29), **g**(**r**) is called *testing function*. The subscripts denote which nanostructure (monomer or dimer) the basis and testing functions belong to, while the superscripts emphasize the order of the basis and testing function. When the testing functions are identical with the basis functions, the testing procedure is called "Galerkin" testing [42]. Though Galerkin testing is accurate and preserves the reciprocal symmetry of Maxwell's equations, it requires eight-fold integrals (a six-fold integral can be seen in Eqs. (28) and (29) and the extra two-fold comes from the evaluation of the Green's function). To ease the computational efforts, instead we pursue the Galerkin testing procedure in the *z* direction and a well-known simpler razor-blade testing procedure (which saves a two-fold integration) in the *horizontal* plane [29]. As a consequence, the testing functions are different from the basis functions and therefore the symmetry of the resultant matrices is weakly disturbed, finally leading to the noticeable discrepancy in Fig. 3(b) between the imaginary parts of $c^{MD}\left(\omega\right)$ and $c^{DM}\left(\omega\right)$.

Since the matrix on the left hand side of (23) describes the coupling between eigenmodes, we call this matrix hereafter the "*coupling matrix*". Extra attention ought to be paid to the fact that although the quantities defined in Eqs. (24)–(27) have the units of Ohms, they do not conform to the conventional definition of impedance in circuit theory, since Eqs. (24)–(27) are obtained by applying the definition of reaction [31] rather than power [44].

On the right hand of Eq. (23), *the coupling between the Y polarized incident field and the current eigenmodes* is modeled as the "voltage" sources driving the loops,

$$e_1^M\left(\omega\right) = \int_{V_M} \mathbf{J}_1^M\left(\mathbf{r}',\omega\right)\cdot\mathbf{E}_{\mathbf{inc}}\left(\mathbf{r},\omega\right)dv, \quad (30)$$

$$e_1^D\left(\omega\right) = \int_{V_D} \mathbf{J}_1^D\left(\mathbf{r}',\omega\right)\cdot\mathbf{E}_{\mathbf{inc}}\left(\mathbf{r},\omega\right)dv. \quad (31)$$

Note that since the net dipolar moment of the quadrupole mode is zero, it is decoupled from the normally incident Y polarized light and the equivalent source driving the "dimer" loop is shorted-circuited, i.e. $e_1^D\left(\omega\right)=0$. Knowing the coupling matrix and excitation in Eq. (23), we can calculate the "currents" $j_1^M\left(\omega\right)$ and $j_1^D\left(\omega\right)$ circulating in the loops (See Fig. 3(d)).

In parallel with Eq. (17), the eigenvalue problem for Eq. (23) is

$$\begin{pmatrix} c^{MM}\left(\omega\right) & c^{MD}\left(\omega\right) \\ c^{DM}\left(\omega\right) & c^{DD}\left(\omega\right)\end{pmatrix}\begin{pmatrix} j_1^M\left(\omega\right) \\ j_1^D\left(\omega\right)\end{pmatrix} = \lambda\left(\omega\right)\begin{pmatrix} j_1^M\left(\omega\right) \\ j_1^D\left(\omega\right)\end{pmatrix}. \quad (32)$$

By solving Eq. (32), the eigenvectors and eigenvalues of the whole structure can be obtained. Remembering Eq. (20), the components of each eigenvector, i.e. $j_1^M\left(\omega\right)$ and $j_1^D\left(\omega\right)$, are the weights of the contributions from the eigenmodes of the constituent monomer and dimer structures to the eigenmode of the whole dolmen structure. Here, the monomer's dipolar mode and the dimer's quadrupolar mode hybridize into the bonding and anti-bonding modes. In the circuit model, the bonding mode indicates the currents in the monomer's loop and the dimer's loop flowing against each other; the anti-bonding mode is equivalent to the currents in the monomer's loop and the dimer's loop flowing along with each other.

#199641 - $15.00 USD Received 17 Oct 2013; revised 27 Nov 2013; accepted 27 Nov 2013; published 10 Dec 2013

The eigenvalues of the hybridized modes can be found as (See the middle graph in Fig. 3(a)),

$$\lambda(\omega)=\frac{\left(\lambda_1^M(\omega)+\lambda_1^D(\omega)\right)\pm\sqrt{\left(\lambda_1^M(\omega)-\lambda_1^D(\omega)\right)^2+4c^{MD}(\omega)c^{DM}(\omega)}}{2}. \quad (33)$$

By comparing the eigenvalues derived from Eq. (33) (see red and green curves in the middle column of Fig. 3(a)) with the eigenvalues directly retrieved from Eq. (17) (see red and green curves in Figs. 2(a) and 2(b) and the light grey curves in the middle column of Fig. 3(a)), we can summarize that Eq. (33) provides a good estimation for the eigenvalues of the L1 and L3 dolmen modes. Furthermore, the resonant wavelengths of the hybridized modes are found at the wavelengths where the imaginary part of their eigenvalues crosses zero, around 850 nm for the bonding mode and around 700 nm for the anti-bonding mode. It can be seen from Fig. 3(d) that at these wavelengths the whole equivalent circuit is at resonance.

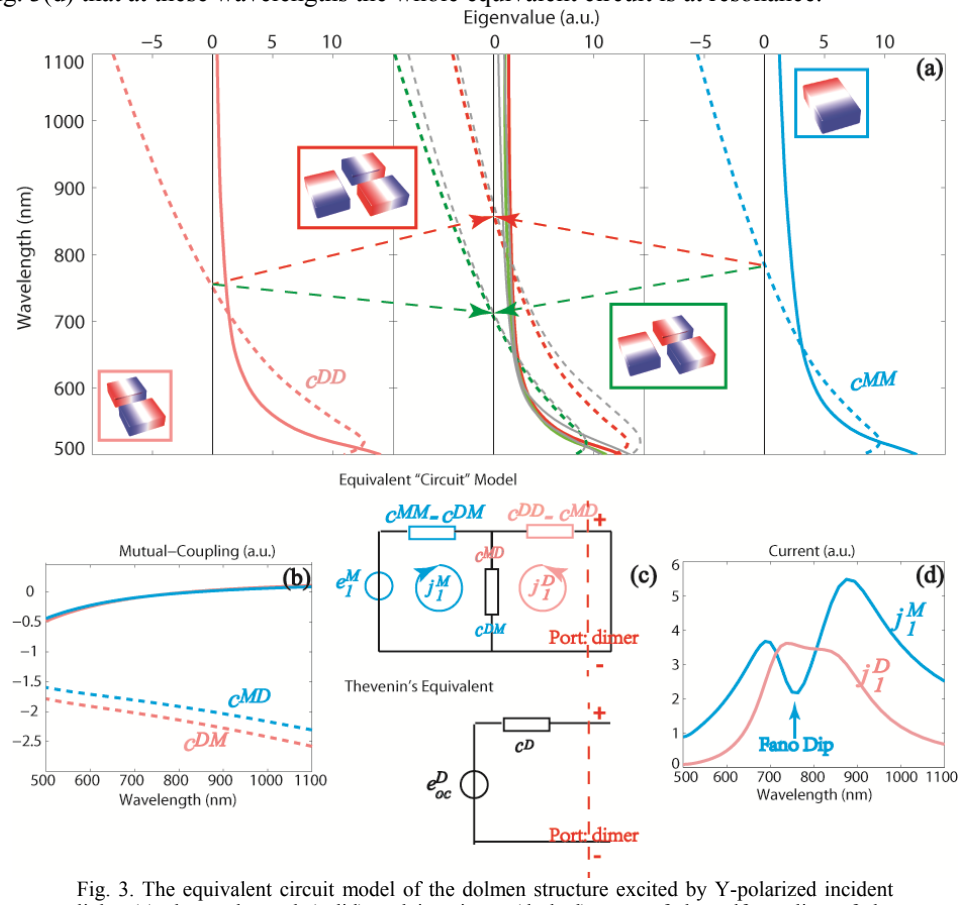

Fig. 3. The equivalent circuit model of the dolmen structure excited by Y-polarized incident light. (a) shows the real (solid) and imaginary (dashed) parts of the self-coupling of the monomer's dipolar mode (cyan, left column), the dolmen's L1 and L3 modes (red and green, resp., middle column), and the dimer's quadrupolar mode (pink, right column). The eigenvalues of the L1 and L3 modes directly extracted as in Eq. (17) (the red and green lines in Figs. 2(a) and 2(b)) are shown as grey lines in (a). The charge density distributions of the dimer's quadrupolar mode, the monomer's dipolar mode, and their hybridized modes are shown in the insets of (a). (b) shows the real (solid) and imaginary (dashed) parts of the mutual coupling. Knowing the self-coupling and mutual coupling, as well as the driving voltage source, an equivalent circuit for the dolmen structure can be constructed as shown in (c). The Thévenin's equivalent of the equivalent circuit is also presented in (c). As a result, the current circulating in each loop can be found as in (d). The reference directions of the currents are shown in (c).

#199641 - $15.00 USD Received 17 Oct 2013; revised 27 Nov 2013; accepted 27 Nov 2013; published 10 Dec 2013

4. Fano resonance in the dolmen structure: a Thévenin's theorem viewpoint

Extra attention needs to be paid to the spectral dip indicated in Fig. 3(d) where the current in the "monomer loop" reaches a minimum. In contrast, the current in the "dimer" loop approaches a maximum. This observation has been attributed to destructive Fano interference of a spectrally overlapping and coupled broad superradiant surface plasmon resonance, i.e. the monomer's dipolar mode, with a narrow subradiant mode, i.e. the dimer's quadrupolar mode [33] and theoretically treated by the Fano model [34] and generalized Fano model [35–39]. Here, from the perspective of Thévenin's theorem [32], we identify the effects of circuit parameters in Eq. (23) on the formation of a Fano resonance. Since the calculation of circuit parameters can be easily integrated into existing Volumetric Method of Moments [27–30] algorithms, such a thorough understanding may open the possibility of utilizing the proposed circuit model in numerically optimizing the asymmetric line shape and facilitating the design of Fano resonance based plasmonic sensing applications [4].

To start, we reformulate the circuit equation describing the "monomer" loop, i.e. the first row of Eq. (23) as,

$$c^{MM}(\omega) j_1^M(\omega) = e_1^M(\omega) - c^{MD}(\omega) j_1^D(\omega). \tag{34}$$

From the equivalent circuit model, we can identify two independent sources on the right-hand side of Eq. (34): 1) the voltage source $e_1^M(\omega)$ imposed by the incident field in the "monomer" loop; 2) the voltage $-c^{MD}(\omega) j_1^D(\omega)$ induced by the current circulating in the "dimer" loop $j_1^D(\omega)$ via the mutual coupling $c^{MD}(\omega)$. Due to the linearity of Maxwell's equations, these two sources can be treated separately.

Firstly, we consider the case in which the dimer is not present and the monomer's dipolar mode is excited by the Y polarized incident wave (See Fig. 4(a1)). This situation is equivalent to open circuit the "dimer" loop (See Fig. 4(a2)). That is to say, the current in the dimer loop is zero,

$$j_1^{D(1)}(\omega) = 0, \tag{35}$$

while due to the imposed source the current in the monomer loop is

$$j_1^{M(1)}(\omega) = \frac{e_1^M(\omega)}{c^{MM}(\omega)}. \tag{36}$$

Further, $j_1^{M(1)}(\omega)$ introduces a voltage $e_{oc}^D(\omega)$ across the ends of disconnected "dimer" loop,

$$e_{oc}^D(\omega) = -c^{DM}(\omega) j_1^{M(1)}(\omega). \tag{37}$$

According to the conventions in circuit theory, this voltage $e_{oc}^D(\omega)$ is called the **"***open-circuit***"** voltage and the ends where the "dimer" loop is cut form a **"***port***"**, further named the **"***dimer port***"**.

Secondly, we remove the incident wave and feed the dimer's quadrupolar mode $\mathbf{J}_1^D(\mathbf{r},\omega)$ with an amplitude $j_1^D(\omega)$ (See Fig. 4(b1)) to excite the monomer's dipolar mode $\mathbf{J}_1^M(\mathbf{r},\omega)$. In the circuit model, this is equivalent to adding a current source at the dimer port (See Fig. 4(b2)). As a result, the current circulating in the "dimer" loop is,

$$j_1^{D(2)}(\omega) = j_1^D(\omega). \tag{38}$$

Due to the electromotive force created by $j_1^{D(2)}(\omega)$, a current $j_1^{M(2)}(\omega)$ is induced in the "monomer" loop,

#199641 - $15.00 USD Received 17 Oct 2013; revised 27 Nov 2013; accepted 27 Nov 2013; published 10 Dec 2013

$$j_1^{M(2)}(\omega) = -\frac{c^{MD}(\omega)}{c^{MM}(\omega)} j_1^{D(2)}(\omega). \tag{39}$$

The input impedance to the dimer port $c^D(\omega)$ can be derived by calculating the ratio of the voltage across the dimer port to the imposed current $j_1^D(\omega)$,

$$c^D(\omega) = c^{DD}(\omega) + c^{DM}(\omega)\left(-\frac{c^{MD}(\omega)}{c^{MM}(\omega)}\right). \tag{40}$$

The "monomer" loop's current $j_1^M(\omega)$ (See Fig. 3(d)), is the sum of the currents introduced by two independent sources,

$$j_1^M(\omega) = j_1^{M(1)}(\omega) + j_1^{M(2)}(\omega). \tag{41}$$

It can be seen from Figs. 4(a3) and 4(b3) that around 800 nm then $j_1^{M(2)}(\omega)$ counter-flows with respect to the current $j_1^{M(1)}(\omega)$. That is to say, in the equivalent circuit (Fig. 3(c)) the source voltage imposed by the source field $e_1^M(\omega)$ is balanced by the electromotive force $-c^{MD}(\omega) j_1^D(\omega)$ due to the mutual coupling from the "dimer" loop. As a result, the voltage drop across the "monomer" loop is approximately zero, the net current minimizes, correspondingly yielding a Fano dip in Fig. 3(d).

By substituting Eq. (41) into the second row of Eq. (23), we can recover the *Thévenin equivalent* of the circuit,

$$e_{oc}^D(\omega) = c^D(\omega) j_1^D(\omega). \tag{42}$$

As shown in Fig. 3(c), the *Thévenin theorem* "seals" the electrical circuit left to the dimer port into a "black box" which contains an open circuit voltage $e_{oc}^D(\omega)$ in series with an equivalent impedance $c^D(\omega)$. Physically, *Thévenin's theorem* selects the dimer's quadrupolar mode as a "port" interfacing the system, which is composed of the dolmen structure and the incident wave, to the "outside" world. The tuning of the dimer's quadupolar mode by, for example, loading the dimer with a different plasmonic material which is equivalent to add an inductive load at the dimer port in the circuit model, can be conducted without considering the detailed electromagnetic properties inside the "port".

The current flowing in the "dimer" loop $j_1^D(\omega)$ is thus the ratio of the open circuit voltage $e_{oc}^D(\omega)$ to the input impedance to the "dimer" port $c^D(\omega)$,

$$j_1^D(\omega) = \frac{e_{oc}^D(\omega)}{c^D(\omega)}. \tag{43}$$

Combining Eqs. (36), (37), and (40) with Eq. (42), Eq. (42) can be simplified as,

$$j_1^D(\omega) = \frac{e_{oc}^D(\omega)}{c^D(\omega)} = \frac{-c^{DM}(\omega) e_1^M(\omega)}{c^{DD}(\omega) c^{MM}(\omega) - c^{MD}(\omega) c^{DM}(\omega)}. \tag{44}$$

In the ideal case where the resonances of the monomer's dipolar and the dimer's quadrupolar mode are degenerate, the imaginary parts of $c^{MM}(\omega)$ and $c^{DD}(\omega)$ cross zero at the same wavelengths. As a result, the denominator of Eq. (43) reaches a minimum and accordingly the current in the dimer loop becomes maximum (See Fig. 3(d) and the pink curves in Fig. 4(b3)).

#199641 - $15.00 USD Received 17 Oct 2013; revised 27 Nov 2013; accepted 27 Nov 2013; published 10 Dec 2013

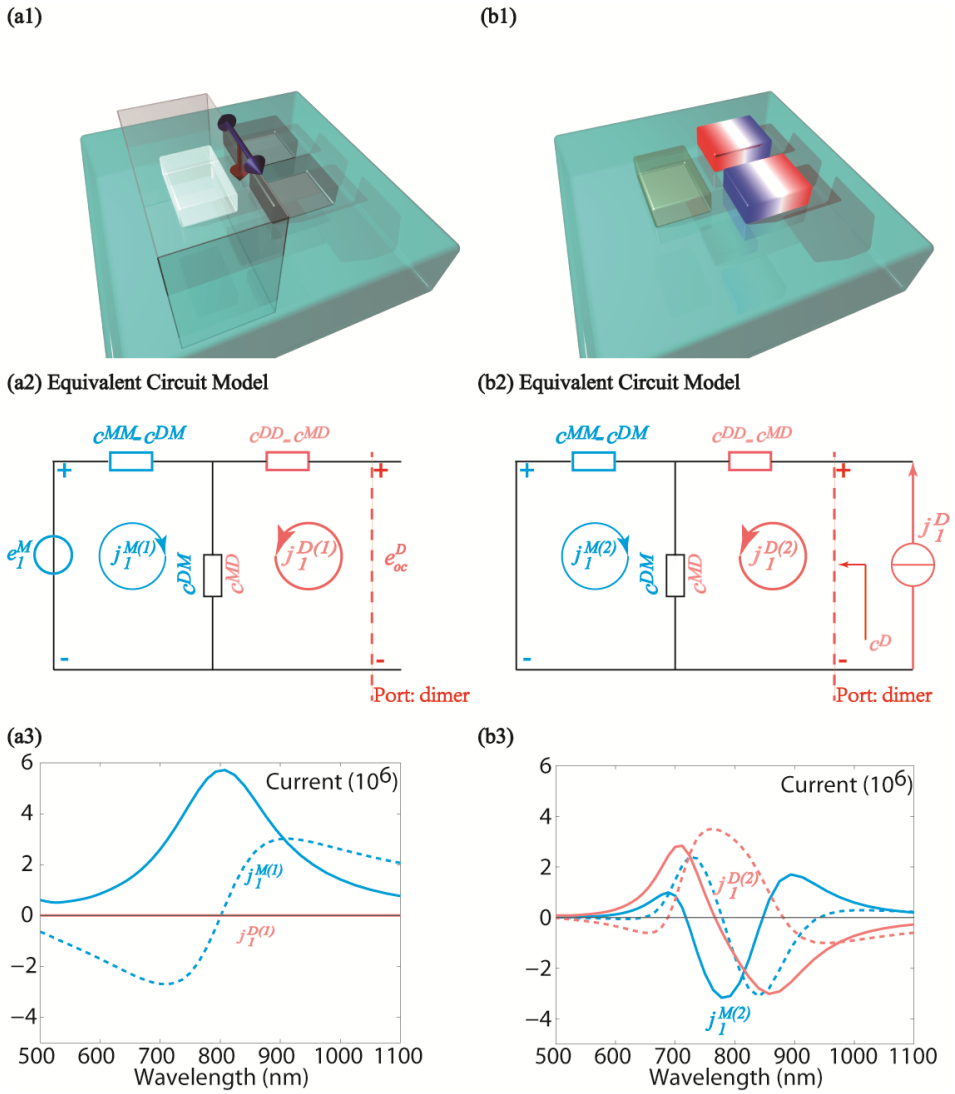

Fig. 4. Illustration of Thévenin's theorem for coupled nanostructures. In (a1), only the monomer is present and excited by an incoming plane wave. The polarization and propagation direction of the incident plane wave are denoted by the blue and red arrows, resp. In (a2), the equivalent circuit model of (a1) is plotted with the open-circuit voltage explicitly defined. (a3) shows the corresponding the real (solid) and imaginary (dashed) parts of the currents circulating in the monomer's loop $j_1^{M(1)}(\omega)$ and the dimer's loop $j_1^{D(1)}(\omega)$. In (b1), the monomer structure is excited by the quadrupolar mode in the dimer structure with an amplitude of $j_1^{D}(\omega)$. The equivalent circuit of (b1) is illustrated in (b2). The real (solid) and imaginary (dashed) parts of the currents in the monomer's loop $j_1^{M(2)}(\omega)$ and the dimer's loop $j_1^{D(2)}(\omega)$ due to the excitation of the quadrupolar mode are plotted in (b3). As in Fig. 3, the monomer loop and its associated quantities are always denoted by the cyan color, while the dimer loop is specified by the pink color.

5. Conclusion

In summary, we propose an approach to characterize the interaction between plasmonic nanostructures by an equivalent circuit model. The eigenvalue problem for a composite

#199641 - $15.00 USD Received 17 Oct 2013; revised 27 Nov 2013; accepted 27 Nov 2013; published 10 Dec 2013

nanoscatterer is first illustrated with a dolmen structure. The effects of the eigenmodes and eigenvalues on the plasmonic response are discussed. By further examining the eigenmodes of the dolmen's composite structures, the monomer and dimer, we boil down the interaction between plasmonic nanostructures to the interaction between their eigenmodes. As an example, the interaction of the monomer's dipolar mode with the dimer's quadrupolar mode is emphasized and summarized in a coupling matrix. Furthermore, an equivalent circuit model is conceived, based on which the plasmonic mode hybridization is elaborated. Last but not least, an equivalent of Thevenin's theorem in circuit theory for plasmonic nanostructures is derived. From this perspective, the well-known Fano dip in the dolmen's spectral response is explained.

It is worth noticing that although the discussion is confined here to the context of two linearly coupled circuits, i.e. a 2 x 2 network, the proposed circuit model can be readily generalized to an N x N network to include the electromagnetic interactions between multiple nanostructures supporting multiple eigenmodes. In this way, the proposed model allows the reuse of many well-established circuit analysis techniques [32] and therefore promises a substantial simplification in future analyses and design of coupled nanoscale plasmonic systems.

Acknowledgments

This work was supported by the Fund for Scientific Research Flanders, Katholieke Universiteit Leuven (GOA), the Flemish Government through Methusalem Funding, the MP1201 COST Action, and UK EPSRC grant EP/G060649/1 and ERC LINASS 320503. N.V. acknowledges the F.W.O. (Flanders) for financial support.